Assessing Transboundary-Local Aerosols Interaction Over Complex Terrain Using a Doppler LiDAR Network

Tao Huang[1] , **Yue Li[2]** , **Jack C. H. Cheng[1]**, **Jim Haywood[3,4]** , **K. K. Hon[5]** , **David H. Y. Lam[5]**, **Olivia S. M. Lee[5]**, **Simone Lolli[6,7]** , **Ewan James O'Connor[8,9]** , **Harry F. Lee[1]**, **Mengya Wang[1]**, and **Steve H. L. Yim[1,2,10,11]**

[1]Department of Geography and Resource Management, The Chinese University of Hong Kong, Hong Kong, China, [2]Institute of Environment, Energy and Sustainability, The Chinese University of Hong Kong, Hong Kong, China, [3]Department of Mathematics, College of Engineering, Mathematics and Physical Science, University of Exeter, Exeter, UK, [4]Met Office, Exeter, Devon, UK, [5]Hong Kong Observatory, Hong Kong, China, [6]CNR-IMAA, Istituto di Metodologie Ambientali, Tito, Italy, [7]Department of Physics, Kent State University (Florence Campus), Kent, OH, USA, [8]Finnish Meteorological Institute, Helsinki, Finland, [9]Department of Meteorology, University of Reading, Reading, Berkshire, UK, [10]Stanley Ho Big Data Decision Analytics Research Centre, The Chinese University of Hong Kong, Hong Kong, China, [11]Asian School of the Environment, Nanyang Technological University, Singapore, Singapore

Abstract Transboundary-local aerosols interaction requires to be comprehensively understood in urban air quality research. A year-long intensive observation of the atmospheric boundary layer (ABL) at multiple sites in Hong Kong was conducted using a four-Doppler Light Detection and Ranging (LiDAR) network with different scanning modes. Results show that heterogeneity of the ABL in terms of mixing layer height and wind shear was induced by orographic topography. Interaction between local and advected aerosol layers during a transboundary air pollution (TAP) episode was identified by the network. During TAP episode, downward transport of transboundary aerosol relied on small scale eddies with weak wind speed in nighttime, while the transport of surface local aerosol to upper level was the dominated process in daytime, but the heterogeneity of the ABL affected by terrain determined the capacity of the mixing, eventually resulting in the opposite transport direction of aerosols in the transboundary-local aerosols interaction.

Plain Language Summary Upper level aerosol transported from remote places brings difficulties to urban air quality forecast. To identify the advected aerosol in the atmospheric boundary layer (ABL) and assess the further impacts after its occurrence, a four-Doppler LiDAR network in Hong Kong was implemented. Upper level advected aerosol layer was captured by the network, and our results show that complex terrain can lead to the spatial differences in the mixing layer height and wind shear, which stand for the characteristics of the ABL. After the advected aerosol arrived at the upper level over Hong Kong, small eddies in the weak wind condition can help to move the aerosol downward to the ground at night. After sunrise, surface accumulated aerosol was driven upward by the turbulent mixing, which was mainly caused by buoyancy. However, the differences in the ABL characteristics affect this upward transport, and finally resulted in two different transport patterns.

1. Introduction

Transboundary air pollution (TAP) is considered as one of the main sources of urban air pollution episodes (Gu & Yim, 2016; Hou et al., 2019; Luo et al., 2018; Shi et al., 2020; Tong et al., 2018; Yim, Gu, et al., 2019; Yim, Hou, et al., 2019). In the atmospheric boundary layer (ABL), transboundary aerosols interact with clouds, turbulence, and local emissions, hence substantially affect local weather and aerosol patterns (Arya, 1995, 1999; Garratt, 1994; Li et al., 2017; Stull, 1988). Transboundary-local aerosols interaction, which is one of sub-grid-scale (SGS) processes in ABL, is significantly influenced by complex topography and the heterogeneity of thermal and dynamic conditions in the ABL. Despite its significant effect on air quality and regional climate, transboundary-local aerosols interaction has yet to be fully understood (X. Huang et al., 2020; Lolli et al., 2019; Qin et al., 2016), thus inducing large uncertainties in climate projection and weather forecasts (Bretherton et al., 2019; Schmidt et al., 2015).

Turbulent transport is a key mechanism in transboundary-local aerosols interaction. Turbulence within ABL is typically generated from buoyancy and wind shear (Stull, 1988). Strong surface heating generates buoyancy that drives surface aerosols up to higher altitudes (Berg et al., 2017; Hogan et al., 2009; Lolli et al., 2019). This process is particularly strong in daytime. Mixing layer height (MLH) is usually utilized to reveal the magnitude of the buoyant transport (Geiß et al., 2017; Y. Liu et al., 2019; Tang et al., 2016; Y. Yang et al., 2019; Zhu et al., 2018). Dynamically, wind shear plays a substantial role in the regulation of aerosol concentration and convective systems (Q. Chen et al., 2015; J. Fan et al., 2009). Weak wind, which is frequently associated with air stagnation, can serve as a critical driving factor to accumulate aerosols near the ground level (Y. Chen et al., 2018; Y. Yang et al., 2019). Meanwhile, if strong wind shear occurs at upper levels, the induced downward transport of momentum can also cause ground-level air pollution (Zhang et al., 2020). Nevertheless, the effects of MLH and wind shear on vertical distribution of aerosols remain unclear.

Complex terrain can influence transboundary-local aerosols. Numerical studies show that terrain affects the development of the inner boundary layer structure (Hon, 2020; H. Liu et al., 2001; Tse et al., 2020) and thus aerosol vertical mixing. Ning et al. (2019) revealed that heavily polluted episodes can be formed due to unfavorable terrain effects. For example, a 4-month observation shows mountain-plain winds had substantial effects on the PM concentration at urban and suburban sites in Beijing (Y. Chen et al., 2018). In Hong Kong, different air motions over urban and suburban areas may result in different levels of air pollutant concentration during heat and polluted days (Yim, 2020). Nevertheless, how the dynamical processes due to terrain effects influence transboundary-local aerosols interaction was seldom explored due to the lack of upper level measurements (Barlow et al., 2017; T. Huang et al., 2020; National Research Council, 2009; Y. Yang et al., 2019; Yim, 2020).

Without upper level measurements, previous studies employed chemical transport models (CTMs) to understand transboundary aerosol effects at regional scale. For example, X. Huang et al. (2020) revealed that long-range transport aerosol can participate in the local aerosol-ABL feedback and eventually amplify the TAP in North and East China. In South China, Hou et al. (2019) applied a numerical model to assess the contributions of different aerosol species in TAP to Pearl River Delta (PRD). While more physical processes have been recently included in numerical models at much higher spatial resolutions, model accuracy has been substantially improved (Bony et al., 2015; McMichael et al., 2020). However, parameterizations of processes in the ABL in numerical models still cannot fully describe the thermal and dynamical processes related to turbulence at urban scale. Large model uncertainties therefore remain and need to be further improved. Since the processes may have significant spatial heterogeneity and are potentially influenced by complex topography (Bretherton et al., 2004; Lopez-Coto et al., 2020; Yuval & O'Gorman, 2020), vertical measurements at multiple sites are required.

This study conducted a year-long observation using a network of four Doppler Light Detection and Ranging (LiDARs), including two units from 3D Real-Time Atmospheric Monitoring System (3DREAMS; Yim, 2020) and another two units operated by the Hong Kong Observatory (HKO) with different scanning modes at urban and suburban areas and at the airport of Hong Kong to assess the effects of thermal and dynamical processes and complex topography on transboundary-local aerosols interaction in the ABL.

2. Materials and Methods

2.1. 3DREAMS and HKIA LiDAR

To understand the effects of terrain on MLH, wind shear, and the consequent impacts on air quality as well as the transboundary-local aerosols interaction, we analyzed the observations from 1-year long range-resolved profiles of aerosol and wind provided by 3DREAMS and HKO. 3DREAMS is a Doppler LiDAR network located in Hong Kong since 2019. 3DREAMS network is now comprised of three 1.5-μm Doppler LiDARs (Halo Photonics Stream Line Scanning Doppler LiDAR system) implemented at the Physical Geography Experimental Station of the Chinese University of Hong Kong (CUHK, 22°24′55.2″N 114°12′44.0″E), King's Park Meteorological Station (KP, 22°18′42.0″N 114°10′20.9″E) and the Hung Shui Kiu Ling Liang Church (HSK, 22°25′41.5″N 113°59′24.8″E). The HSK LiDAR was operated from June 2020, which is outside the study period of this work. This study used the LiDARs at CUHK and KP only, and their locations are

shown in Figure S1. In addition, data from two units of long-range, coherent pulsed Doppler LIDARs (Mitsubishi Electric with 1.5-μm laser beams) operated by HKO at the Hong Kong International Airport (HKIA) were analyzed in this study (Figure S1). Detailed settings are provided in the Supporting Information (SI).

2.2. Vertical Distribution of Aerosol, Wind Patterns, and Turbulence

The attenuated backscatter coefficient (β) can be directly retrieved from Doppler LiDAR's measurement. Nevertheless, considering the impact of focus length, we derived the validated β (β') with a known telescope focus function retrieved from the same Halo Photonics StreamLine LiDAR and a synergistic ceilometer measurement in Finland (Pentikäinen et al., 2020). Following this, the maximum negative gradient of β' was utilized to detect the top of the MLH (Tang et al., 2016). Vertical velocity (w) was obtained directly from the vertically pointing Stare mode at 1.13 s and 30 m resolution. Horizontal wind speed and direction were derived from velocity azimuth displays mode every 10 minutes. Measurements with the signal intensities lower than 1.01 were discarded (T. Huang et al., 2020). After that, vertical wind shear (VWS) intensity was defined within the derived MLH as:

$$\text{VWS} = \frac{\left(\Delta u^2 + \Delta v^2\right)^{1/2}}{\Delta Z},$$

where u and v are zonal and meridional wind components of horizontal wind, respectively. ΔZ stands for the difference between two adjacent layers, which is 30 m in this study. The calculation of turbulent mixing, dissipation rate of turbulent kinetic energy (TKE) ϵ, and friction velocity u_* can be referred in SI.

2.3. Surface Level Observation of Meteorology and Aerosol Concentration

Surface level meteorological data was obtained from the website of HKO (https://www.hko.gov.hk/en/cis/climat.htm). All the days with rainfall in 2019 were excluded in this study. For surface aerosol concentration, hourly surface $PM_{2.5}$ concentration data was obtained from two air quality monitoring stations near our 3DREAMS LiDARs: Shatin (near CUHK) and Sham Shui Po (near KP) (https://www.aqhi.gov.hk/en.html). To determine the low and high surface aerosol concentration days, we normalized the daily concentration by their monthly mean value (Wang et al., 2018). Following this, the ¼ and ¾ quantiles were denoted clean days and pollution episodes, respectively.

2.4. Back Trajectory

HYbrid Single-Particle Lagrangian Integrated Trajectory (HYSPLIT) was applied to simulate air mass trajectories for identifying the origin of the air mass. The HYSPLIT was configured to perform back trajectory calculations at 1,500 m above two 3DREAMS LiDAR sites: KP and CUHK for 24 h using the meteorological data of the Global Data Assimilation System (GDAS) at the spatial resolution of 0.25°. The specific information of all the data utilized in this study can be found in Table S1.

3. Results

3.1. Year-Long Observation of MLH and Wind Shear Under Terrain Effects

Hourly MLHs at CUHK and KP were calculated in winter (DJF), spring (MAM), summer (JJA), and fall (SON) according to the maximum negative gradient of β'. Figure 1a shows that the highest seasonal mean MLH occurred in JJA (~1,300 m), whereas the lowest mean MLH occurred in DJF (~900 m). Meanwhile, despite the fact that surface air temperature at these two locations reveals that heating capacity was higher at KP than at CUHK (Table S2), MLHs over CUHK were always ~70 m higher than those over KP in the whole year. Figure 1b shows that the magnitude of column mean wind shear at CUHK was weaker. For mean values, the smallest difference in wind shear between the two sites (0.01 s^{-1}) occurred in winter, and the largest (0.03 s^{-1}) occurred in spring, suggesting that VWS was not the main factor that contributed to the higher MLH at CUHK. Yim (2020) analyzed wind patterns in HK and reported that CUHK was dominated
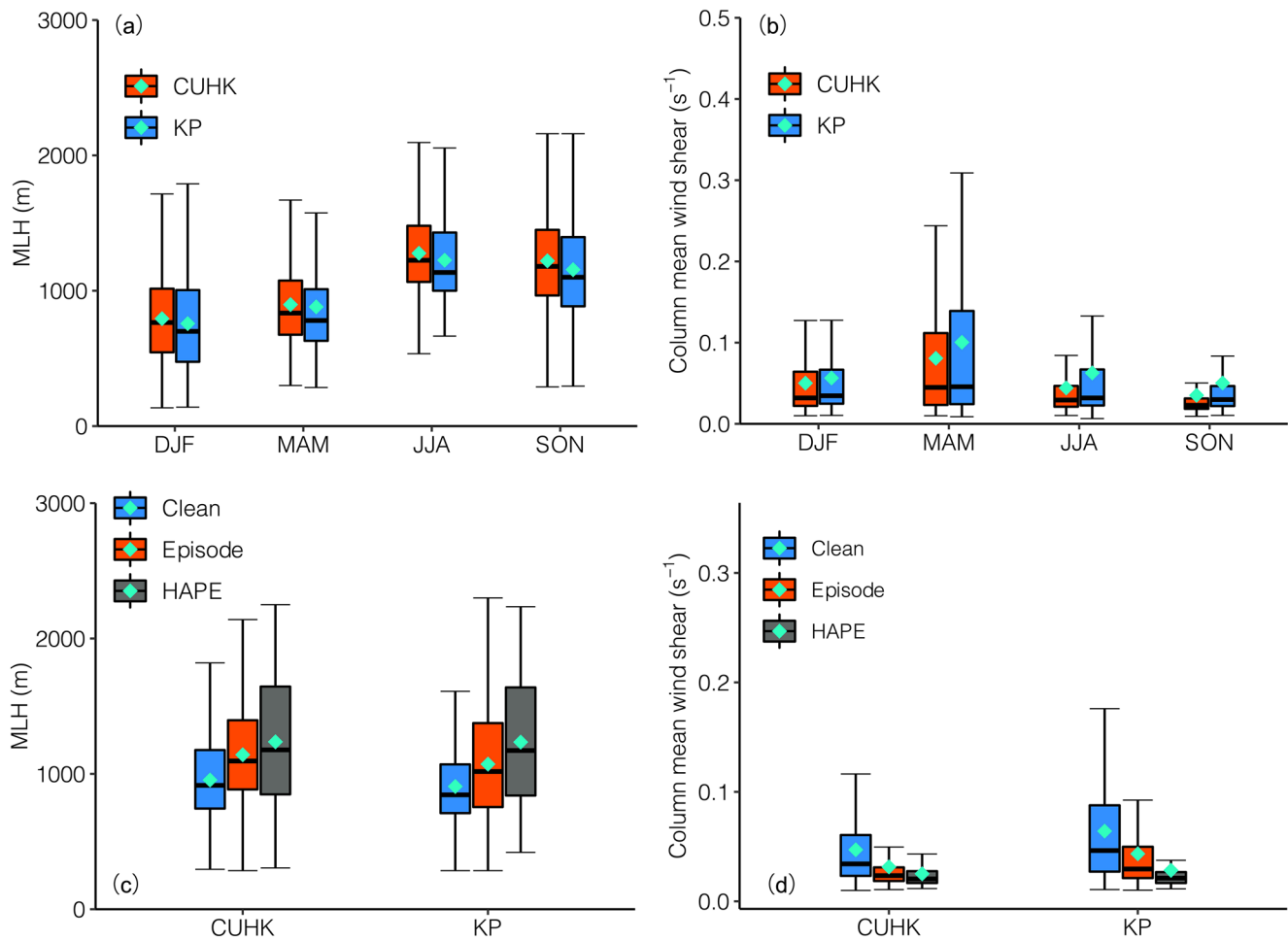
Figure 1. Year-long boxplot of (a) Seasonal variation of the MLH (m); (b) Seasonal variation of the column mean of wind shear (s^{-1}) within the MLH (m); (c) Station differences of the MLH (m) during clean days, episodes and HAPE days and (d) Station differences of the column mean of wind shear (s^{-1}) within the MLH (m) during clean days, episodes and HAPE days. Green dots represent the mean value. HAPE, Heavy-Air-Polluted-Episode; MLH, mixing layer height.

by updrafts below ~700 m. Overall, it is inferred that the higher MLH at CUHK was mainly due to updrafts generated by the surrounding valley that enhanced vertical mixing.

Surface aerosol concentration was represented by the $PM_{2.5}$ concentration measured at two air quality monitoring stations (SSP and ST) near the 3DREAMS LiDAR sites (Figure S1). Clean days and pollution episodes were classified in Section 2. Seven extreme polluted episodes (Table S3) with normalized concentration higher than 90% percentile (defined as Heavy-Air-Polluted-Episode [HAPE]) were also compared to different polluted regimes. In Figure 1c, clean days were determined with lower mean MLH in urban and suburban areas, while in HAPE, the mean MLH was higher. However, the observation of wind shear shows that heavily polluted days were accompanied by low wind shear (Figure 1d), which is consistent with the statistical result that high aerosol loading in 2019 was overall related to low wind shear conditions no matter at which height and in which season (Figure S4). These results help us to confirm that strong wind shear is critical for aerosol dispersion.

3.2. Recognition of Transboundary Aerosol Layer From LiDAR Observation

Detailed long-range transport processes were captured and recognized by the four-LiDAR network. In a 48-h continuous episode (October 1–2) during the HAPE days, upper level wind profiles from 3DREAM LiDARs at KP and CUHK show that an abrupt change of wind direction from northwest to northeast (0°–45°) took place at the altitude of 1,425 m at 18:20 Hong Kong Time (HKT) over CUHK, whereas the same wind
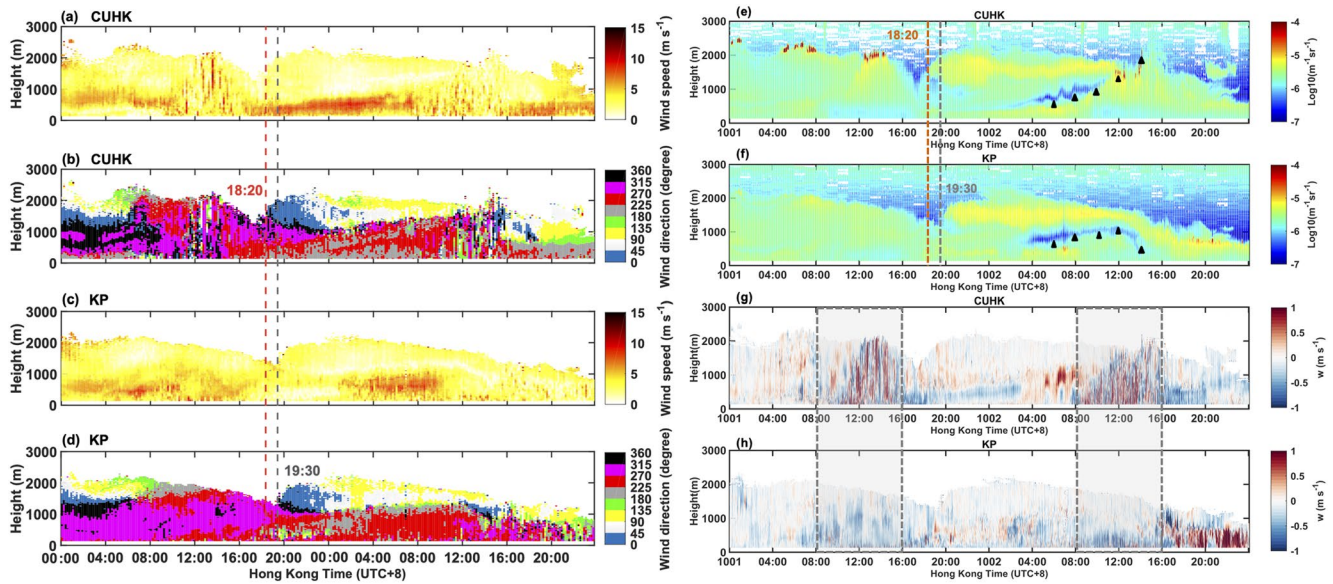
Figure 2. (a–d) Upper level wind profiles of wind speed (m s^{-1}) and direction (°) over CUHK (a–b) and KP (c–d) during the episode. Dash lines depict the occurrence of southeast wind (0°–45°) over CUHK and KP. (e–h) Upper level aerosol and convection patterns over CUHK and KP during the episode. Dash lines in (e) and (f) stand for the occurrence of transboundary aerosol over CUHK and KP. Two gray boxes in (g) and (h) represent the dramatic developing time (08:00 to 16:00) of the ABL. ABL, atmospheric boundary layer.

pattern occurred at 19:30 HKT over KP at the same altitude (Figures 2b and 2d). The wind speed at 1,425 m over CUHK and KP during the time period was 2.8 and 2.1 m s^{-1}, respectively, while the distance between these two sites is ~10 km (Figure S1). The wind speed and direction, and the distance between the two sites suggest that air mass transported from CUHK to KP along the northeast-southwest direction. Figure S5 shows that the result was confirmed by back trajectory analysis before 00:00 HKT October 2 at these two sites (W. Fan et al., 2019).

The wind patterns at the upper level provide a direct observation of the wind condition for TAP episodes within the ABL. To further confirm the measurements of upper level wind profiles at CUHK and KP, the wind measurements at HKIA were analyzed. HKIA is located at a similar latitude as KP but ~26 km away from KP in the east (Figure S1). Figure 3g shows the positions and azimuths of the two LiDARs. Figure 3h depicts the quasi-real vertical profile of horizontal wind at the intersection retrieved from the two HKIA LiDARs. We note that the direct RHI scan can measure radial velocity at altitudes higher than 750 m; nevertheless, the highest level of wind profile that can be retrieved at the intersection of the two HKIA LiDARs is 750 m (Ng & Hon, 2020). Figure 3h shows that enhanced southwesterly wind started to occur at around 19:00 at low level on October 1, which was consistent with the low level wind profiles at KP and CUHK. In Figures 3a–3f, positive velocities represent that wind goes away from the LiDAR, whereas the negative values stand for the air parcels that come toward the LiDAR. The measurement of HKG1 (Figures 3a–3c) shows that the enhancement of westerly wind occurred lower than ~1,400 m, starting from 19:00 with positive radial velocities (from west to east). However, the opposite direction of radial velocities (from east to west) was observed in the upper level, indicating that wind flow at upper levels came from east. The color shift from blue to red observed in HKG2 from 18:00 to 19:00 indicates the prevailing northerly wind at the upper level. Combining the results of the two LiDARs, we can confirm that wind came from northeast at 1425 m.

3.3. Transboundary-Local Aerosols Interaction and Heterogeneity of the ABLs

β' patterns at CUHK and KP (Figures 2e and 2f) show that residual aerosols from the previous day were the primary source of pollution from 00:00 to 08:00 on October 1 (HKT). The relatively larger updrafts (>0.3 m s^{-1}) at CUHK led to the intermittent occurrence of shallow clouds at ~2,000 m. During the daytime on October 1, substantial convective mixing was observed at CUHK, while downdrafts were dominated at
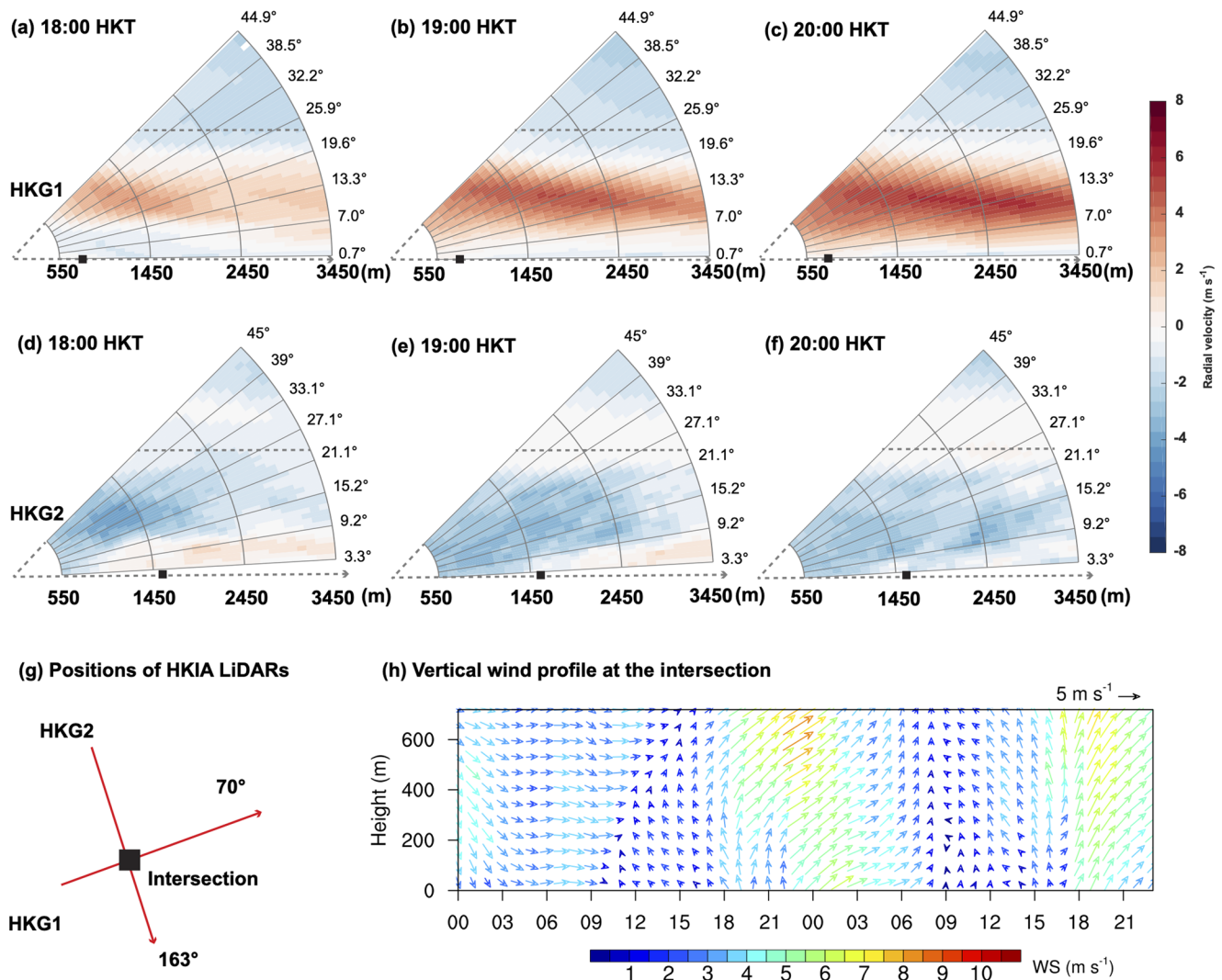
Figure 3. Wind profiles derived from two HKIA LiDARs operating in RHI mode during the episode. (a–c) are the wind profiles from HKG1 at 18:00, 19:00, and 20:00 on October 1 HKT, respectively. Black squares represent the intersection of two scanning paths. Gray horizontal lines stand for the altitude of 1,425 m. Positive radial velocity means winds go away from the LiDAR. (d–f) are the wind profiles from HKG2 at 18:00, 19:00, and 20:00 on October 1 HKT, respectively. (g) is the intersection (black square) position derived from two HKIA LiDARs scanning paths and (h) is the quasi-real vertical profile of horizontal wind (m s^{-1}) at the intersection retrieved from the two LiDARs. HKIA, Hong Kong International Airport; HKT, Hong Kong Time; LiDAR, Light Detection and Ranging.

KP, but the atmosphere was also mixed there. The aerosol patterns at this time show that the diurnal variation of aerosol distribution at CUHK was more evident than that over KP, meanwhile the lower layers (<500 m) were cleaner at CUHK (<−5.7 log10 [m^{-1} sr^{-1}]) than at KP, indicating a better dispersion capacity of local aerosol at CUHK. This process is the typical local aerosol dispersion characteristics in a convective ABL (Arya, 1999).

Substantially high aerosol loading larger than −5.2 log10 (m^{-1} sr^{-1}) occurred at 18:20 on October 1 (HKT) over CUHK at 1,425 m above the ground level (Figure 2e), and then started to occur at KP at the same altitude at 19:00 (HKT) on the same day (Figure 2f), which was similar to changes in wind profiles. Afterward, the transboundary aerosol layer was maintained at this altitude over Hong Kong until October 2. After sunrise (06:00, October 2 HKT), when the mixing layer started to develop (black triangles in Figures 2e and 2f), substantial differences in MLH were observed at the two sites. At CUHK, due to the intense turbulent mixing during the mixing layer development period, local aerosol was driven up to over 1,500 m by buoyancy at 12:00 (HKT), and then well mixed with upper level transboundary aerosol, which was revealed by the disappearance of the boundary between two aerosol sources. However, the separation between transboundary

aerosols and local aerosols was relatively clear because the development of mixing layer over KP was not as dramatic as the one over CUHK. It should be noted that the MLH was much lower at KP (1,065 m) than at CUHK especially at 12:00 (HKT). The MLH at KP even dropped to 555 m at 14:00 (HKT), which was nearly 3.6 times lower than that over CUHK (2,025 m). It can be summarized that at CUHK the local pollution from the surface mixed upwards owing to the strong diurnal cycle of MLH, while at KP the elevated transboundary pollution layer transported downward after the diurnal cycle decayed. Previous study (Yim, 2020) found that KP was dominated by downdrafts within the whole ABL, which was also confirmed in this study. Considering the locations of these two sites, all the results indicate that KP has a marine ABL structure, while CUHK has a terrestrial ABL structure.

To further assess the transboundary-local aerosols interaction from a dynamical perspective, the correlation between turbulence patterns within the ABL and surface aerosol concentrations (PM$_{2.5}$ concentration) was explored. The dissipation rate of TKE (ϵ) at each layer was calculated to represent the homogenous and isotropic turbulence with different length scales in the local-transboundary aerosol interaction, while turbulent mixing ($\sigma_w^2(z)$) was utilized to represent convective transport due to the buoyancy. The R value is the correlation coefficient between the layer diagnostic turbulence and the surface aerosol concentration. Figures S6a and S6c show that before the transboundary aerosol arrived, more significant negative R values (< -0.5) occurred over CUHK compared to KP. The negative values show the opposite relationship between turbulence and surface aerosol, indicating that turbulence generated by the surrounding terrain at CUHK enhanced aerosol dispersion. However, after the occurrence of transboundary aerosol over Hong Kong, R values turned to be positive ($R > 0.39$) at CUHK (Figures S6b and S6d), revealing that turbulence transported the transboundary aerosol down to the ground. Figure S6b shows that at CUHK, most significantly positive correlation occurred between ~750 and ~1,100 m. The ϵ pattern in Figure S7a shows that small eddies with smaller length scales at this level during nighttime contributed to the downward transport of the transboundary aerosol, while the stronger horizontal wind speed (>7 m s^{-1}) at low altitude (Figure 2a) reduced the small eddies, making the correlation at lower level not significant. Figure S6d reveals that turbulent mixing developed from the surface level was the main contributor of transporting the upper level aerosol to the ground, which also can be seen in Figure S7b. The more significantly negative correlation at KP should be due to the occurrence of updrafts from ~200 up to ~2,000 m between 18:00, October 1 and 02:00, October 2 (HKT).

4. Discussion

The results of the ABL characteristics are consistent with the results derived from Micro Pulse LiDAR (MPL) at Yuen Long (Su et al., 2017; D. Yang et al., 2013), another residential area in the northwest part of Hong Kong where air pollution episodes occur frequently (Lee et al., 2002). It should be noted that MPL is capable of providing vertical profiles of extinction coefficient and backscatter coefficient, whereas our Doppler LiDARs can provide vertical profiles of both backscatter coefficient and wind. The data pair can support an in-depth analysis of transboundary-local aerosols interaction. It is the first time that spatial variation of ABL has been explored in Hong Kong. Although KP is located in the urban area, the characteristics of marine ABL structure are evident. The heterogeneity of the ABLs should be primarily due to terrain effects at CUHK, which makes the ABL structure at CUHK show terrestrial characteristics with a significant diurnal variation. This emphasizes that the terrain effects on the ABL cannot be ignored. Different from other studies that used multiple LiDARs to measure the regional-scale campaigns within the same synoptic background, this study concentrated on an episode but with complicated surface conditions, which may substantially affect the air pollution regime locally. For wind shear, even though KP has a stronger dynamical mixing capacity due to surface resistance induced by its surrounding high-rise building morphology (Text S2; Figure S2-S3), the buoyancy-driven capacity restricts the aerosol dispersion in daytime. Y. Yang et al. (2019) and Zhang et al. (2020) have revealed that weak wind shear is beneficial for local aerosol accumulation while strong wind shear can help transport upper level aerosol to the ground level, but their studies have yet assessed the influence of the ABL characteristic on the vertical transport. By employing the four-LiDAR network, this study found that, in the studied episode, marine ABL cannot drive local surface aerosols to mix with the upper level transboundary aerosols, whereas the mixing of the surface and transboundary aerosols can happen within terrestrial ABL.

This study has captured a 48-h continuous episode with two states of atmosphere: Local aerosol only and transboundary-local aerosols interaction. Luo et al. (2018) investigated TAP in Hong Kong, but the direct observation was restricted to the ground level, while Lam et al. (2005) and Yim, Gu et al. (2019) employed modeling including numerical simulation and back trajectories. Even though TAP signals were identified using the changes of ground-level concentration and wind speed and direction from in-situ measurements or models, real-time monitoring of TAP still remains challenging. This study has captured the real-time up-per level aerosol and wind changes by using four LiDARs at three different stations using different scanning modes. In this case, TAP took place within very short temporal and spatial scales, which cannot be easily captured by mesoscale modeling. Furthermore, the two 3DREAMS LiDARs were designed to be established at a certain path (northeast to the downtown of Hong Kong), which helps to identify the frequent occur-rence of short-term TAP, and the upper level wind can be inter-compared at three locations. In our following studies, we will further pay attention to another path (northwest to the downtown) using the newly estab-lished 3DREAMS LiDAR at Yuen Long, northwest of Hong Kong. Terrain-induced heterogeneity of the ABL substantially affected this process by the generated turbulence, which cannot be revealed by simple MLH and wind shear analysis. During nighttime, when the wind speed is weak, the downward transport of transboundary aerosol relies on small-scale eddies, while strong wind speed can repel this process. In daytime, the transport of surface local aerosol to upper level is the dominated process, but the heterogeneity of the ABL affected by terrain determined the capacity of the mixing. The accuracy of two key parameters (Dissipation rate of TKE and Turbulent mixing) relies on the high-time resolution observation of vertical velocity, which can be totally ensured by our 3DREAMS LiDAR network. Even though large uncertainties still remain as the case is relatively short in time due to only 1-year observation and the statistical method, the substantial difference in the aerosol profiles can also show the capability of the LiDAR network for air quality monitoring, especially for TAP monitoring.

5. Conclusions

In this study, transboundary-local aerosols interaction was first analyzed by exploring a year-long observa-tion of ABL at three sites (CUHK, KP, and HKIA) in Hong Kong using four Doppler LiDARs with different scanning modes. Our results show that the topography substantially contributed to the heterogeneity of the ABL. MLH at the suburban CUHK site was higher ($\sim$70 m) than that at the urban KP site even though surface heating was stronger at the urban site. The orographic terrain at CUHK had substantial effect to generate updrafts to $\sim$700 m above ground, enhancing the vertical mixing, thus resulting in a higher MLH. In terms of wind shear, due to the higher surface resistance of the urban surface, the magnitude of wind shear was always higher at KP within the ABL. Low wind shear occurred when wind came from southwest Hong Kong because of its relatively open surroundings. During the studied TAP episode, an abrupt change of wind direction from northwest to northeast (0°–45°) occurred at the upper level has been considered as the critical wind condition for the transboundary aerosol. It took $\sim$70 minutes to transport the advected aerosols from CUHK to KP from the direction of northeast-southwest. The signal was also confirmed by two HKIA LiDARs performing an RHI scan. The heterogeneity of the ABLs was also confirmed at CUHK and KP according to aerosol and convection patterns in the episode. An aerosol stratified ABL structure at KP with significant downdrafts indicates a marine ABL at KP, while terrestrial ABL structure is more evident at CUHK. Correlations between turbulence patterns within the ABL and surface aerosol concentration show that downward transport of transboundary aerosol relied on small scale eddies due to weak wind speed in nighttime, while the transport of surface local aerosol to upper level was the dominated process in daytime, but the heterogeneity of the ABL affected by terrain determined the capacity of the mixing, eventually resulting in the opposite transport direction of aerosols in the ABL. Results indicate that terrain-induced heterogeneity of the ABL substantially affected transboundary-local aerosols interaction.

Data Availability Statement

Surface metrological data sets in Hong Kong are available at Hong Kong Observatory's website: https://www.hko.gov.hk/en/cis/climat.htm. PM$_{2.5}$ concentrations data sets can be obtained from Hong Kong Envi-ronmental Protection Department: https://www.aqhi.gov.hk/en.html. Processed 3DREAMS LiDAR data set and HKIA LiDAR data sets can be obtained in the repository: https://figshare.com/s/78e928f29c57ff86b5ee

References

Arya, S. P. (1995). Atmospheric boundary layer and its parameterization. In J. E. Cermak, A. G. Davenport, E. J. Plate, & D. X. Viegas (Eds.), *Wind climate in cities* (pp. 41–66). Springer. https://doi.org/10.1007/978-94-017-3686-2_3

Arya, S. P. (1999). *Air pollution meteorology and dispersion*. Oxford University Press.

Barlow, J., Best, M., Bohnenstengel, S. I., Clark, P., Grimmond, S., Lean, H., et al. (2017). Developing a research strategy to better understand, observe, and simulate urban atmospheric processes at kilometer to subkilometer scales. *Bulletin of the American Meteorological Society*, *98*(10), ES261–ES264. https://doi.org/10.1175/BAMS-D-17-0106.1

Berg, L. K., Newsom, R. K., & Turner, D. D. (2017). Year-long vertical velocity statistics derived from Doppler Lidar data for the continental convective boundary layer. *Journal of Applied Meteorology and Climatology*, *56*(9), 2441–2454. https://doi.org/10.1175/JAMC-D-16-0359.1

Bony, S., Stevens, B., Frierson, D. M. W., Jakob, C., Kageyama, M., Pincus, R., et al. (2015). Clouds, circulation and climate sensitivity. *Nature Geoscience*, *8*(4), 261–268. https://doi.org/10.1038/ngeo2398

Bretherton, C. S., McCaa, J. R., & Grenier, H. (2004). A new parameterization for shallow cumulus convection and its application to marine subtropical cloud-topped boundary layers. Part I: Description and 1D results. *Monthly Weather Review*, *132*(4), 864–882. https://doi.org/10.1175/1520-0493(2004)132<0864:ANPFSC>2.0.CO;2

Bretherton, C. S., McCoy, I. L., Mohrmann, J., Wood, R., Ghate, V., Gettelman, A., et al. (2019). Cloud, aerosol, and boundary layer structure across the Northeast Pacific Stratocumulus-Cumulus transition as observed during CSET. *Monthly Weather Review*, *147*(6), 2083–2103. https://doi.org/10.1175/MWR-D-18-0281.1

Chen, Q., Fan, J., Hagos, S., Gustafson, W. I., & Berg, L. K. (2015). Roles of wind shear at different vertical levels: Cloud system organization and properties. *Journal of Geophysical Research: Atmospheres*, *120*(13), 6551–6574. https://doi.org/10.1002/2015JD023253

Chen, Y., An, J., Sun, Y., Wang, X., Qu, Y., Zhang, J., et al. (2018). Nocturnal low-level winds and their impacts on particulate matter over the Beijing Area. *Advances in Atmospheric Sciences*, *35*(12), 1455–1468. https://doi.org/10.1007/s00376-018-8022-9

Fan, J., Yuan, T., Comstock, J. M., Ghan, S., Khain, A., Leung, L. R., et al. (2009). Dominant role by vertical wind shear in regulating aerosol effects on deep convective clouds. *Journal of Geophysical Research*, *114*(D22), D22206. https://doi.org/10.1029/2009JD012352

Fan, W., Qin, K., Xu, J., Yuan, L., Li, D., Jin, Z., & Zhang, K. (2019). Aerosol vertical distribution and sources estimation at a site of the Yangtze River Delta region of China. *Atmospheric Research*, *217*, 128–136. https://doi.org/10.1016/j.atmosres.2018.11.002

Garratt, J. (1994). Review: The atmospheric boundary layer. *Earth-Science Reviews*, *37*(1–2), 89–134. https://doi.org/10.1016/0012-8252(94)90026-4

Geiß, A., Wiegner, M., Bonn, B., Schäfer, K., Forkel, R., Schneidemesser, E. V., et al. (2017). Mixing layer height as an indicator for urban air quality? *Atmospheric Measurement Techniques*, *10*(8), 2969–2988. https://doi.org/10.5194/amt-10-2969-2017

Gu, Y., & Yim, S. H. L. (2016). The air quality and health impacts of domestic trans-boundary pollution in various regions of China. *Environment International*, *97*, 117–124. https://doi.org/10.1016/j.envint.2016.08.004

Hogan, R. J., Grant, A. L. M., Illingworth, A. J., Pearson, G. N., & O'Connor, E. J. (2009). Vertical velocity variance and skewness in clear and cloud-topped boundary layers as revealed by Doppler Lidar. *Quarterly Journal of the Royal Meteorological Society*, *135*(640), 635–643. https://doi.org/10.1002/qj.413

Hon, K.-K. (2020). Predicting low-level wind shear using 200-m-resolution NWP at the Hong Kong International Airport. *Journal of Applied Meteorology and Climatology*, *59*(2), 193–206. https://doi.org/10.1175/JAMC-D-19-0186.1

Hou, X., Chan, C. K., Dong, G. H., & Yim, S. H. L. (2019). Impacts of transboundary air pollution and local emissions on $PM_{2.5}$ pollution in the Pearl River Delta region of China and the public health, and the policy implications. *Environmental Research Letters*, *14*(3), 034005. https://doi.org/10.1088/1748-9326/aaf493

Huang, T., Yim, S. H., Yang, Y., Lee, O. S., Lam, D. H., Cheng, J. C., & Guo, J. (2020). Observation of turbulent mixing characteristics in the typical daytime cloud-topped boundary layer over Hong Kong in 2019. *Remote Sensing*, *12*(9), 1533. https://doi.org/10.3390/rs12091533

Huang, X., Ding, A., Wang, Z., Ding, K., Gao, J., Chai, F., & Fu, C. (2020). Amplified transboundary transport of haze by aerosol-boundary layer interaction in China. *Nature Geoscience*, *13*, 1–434. https://doi.org/10.1038/s41561-020-0583-4

Lam, K. S., Wang, T. J., Wu, C. L., & Li, Y. S. (2005). Study on an ozone episode in hot season in Hong Kong and transboundary air pollution over Pearl River Delta region of China. *Atmospheric Environment*, *39*(11), 1967–1977. https://doi.org/10.1016/j.atmosenv.2004.11.023

Lee, S. C., Chiu, M. Y., Ho, K. F., Zou, S. C., & Wang, X. (2002). Volatile organic compounds (VOCs) in urban atmosphere of Hong Kong. *Chemosphere*, *48*(3), 375–382. https://doi.org/10.1016/S0045-6535(02)00040-1

Li, Z., Guo, J., Ding, A., Liao, H., Liu, J., Sun, Y., et al. (2017). Aerosol and boundary-layer interactions and impact on air quality. *National Science Review*, *4*(6), 810–833. https://doi.org/10.1093/nsr/nwx117

Liu, H., Chan, J. C. L., & Cheng, A. Y. S. (2001). Internal boundary layer structure under sea-breeze conditions in Hong Kong. *Atmospheric Environment*, *35*(4), 683–692. https://doi.org/10.1016/S1352-2310(00)00335-6

Liu, Y., Tang, G., Zhou, L., Hu, B., Liu, B., Li, Y., et al. (2019). Mixing layer transport flux of particulate matter in Beijing, China. *Atmospheric Chemistry and Physics*, *19*(14), 9531–9540. https://doi.org/10.5194/acp-19-9531-2019

Lolli, S., Khor, W. Y., Matjafri, M. Z., & Lim, H. S. (2019). Monsoon season quantitative assessment of biomass burning clear-sky aerosol radiative effect at surface by ground-based Lidar observations in Pulau Pinang, Malaysia in 2014. *Remote Sensing*, *11*(22), 2660. https://doi.org/10.3390/rs11222660

Lopez-Coto, I., Hicks, M., Karion, A., Sakai, R. K., Demoz, B., Prasad, K., & Whetstone, J. (2020). Assessment of planetary boundary layer parameterizations and urban heat island comparison: Impacts and implications for tracer transport. *Journal of Applied Meteorology and Climatology*, *59*(10), 1637–1653. https://doi.org/10.1175/JAMC-D-19-0168.1

Luo, M., Hou, X., Gu, Y., Lau, N.-C., & Yim, S. H.-L. (2018). Trans-boundary air pollution in a city under various atmospheric conditions. *The Science of the Total Environment*, *618*, 132–141. https://doi.org/10.1016/j.scitotenv.2017.11.001

McMichael, L. A., Yang, F., Marke, T., Löhnert, U., Mechem, D. B., Vogelmann, A. M., et al. (2020). Characterizing subsiding shells in shallow cumulus using Doppler Lidar and large-eddy simulation. *Geophysical Research Letters*, *47*(18), e2020GL089699. https://doi.org/10.1029/2020GL089699

National Research Council. (2009). *Observing weather and climate from the ground up: A nationwide network of networks*. https://doi.org/10.17226/12540

Ng, C. W., & Hon, K. K. (2020). Fast dual-Doppler LiDAR retrieval of boundary layer wind profile. *Weather*. https://doi.org/10.1002/wea.3800

Ning, G., Yim, S. H. L., Wang, S., Duan, B., Nie, C., Yang, X., et al. (2019). Synergistic effects of synoptic weather patterns and topography on air quality: A case of the Sichuan basin of China. *Climate Dynamics*, *53*(11), 6729–6744. https://doi.org/10.1007/s00382-019-04954-3

Pentikäinen, P., O'Connor, E. J., Manninen, A. J., & Ortiz-Amezcua, P. (2020). Methodology for deriving the telescope focus function and its uncertainty for a heterodyne pulsed Doppler Lidar. *Atmospheric Measurement Techniques*, *13*(5), 2849–2863. https://doi.org/10.5194/amt-13-2849-2020

Qin, K., Wu, L., Wong, M. S., Letu, H., Hu, M., Lang, H., et al. (2016). Trans-boundary aerosol transport during a winter haze episode in China revealed by ground-based Lidar and CALIPSO satellite. *Atmospheric Environment*, *141*, 20–29. https://doi.org/10.1016/j.atmosenv.2016.06.042

Schmidt, J., Ansmann, A., Buehl, J., & Wandinger, U. (2015). Strong aerosol-cloud interaction in altocumulus during updraft periods: Lidar observations over central Europe. *Atmospheric Chemistry and Physics*, *15*(18), 10687–10700. https://doi.org/10.5194/acp-15-10687-2015

Shi, C., Nduka, I. C., Yang, Y., Huang, Y., Yao, R., Zhang, H., et al. (2020). Characteristics and meteorological mechanisms of transboundary air pollution in a persistent heavy $PM_{2.5}$ pollution episode in Central-East China. *Atmospheric Environment*, *223*, 117239. https://doi.org/10.1016/j.atmosenv.2019.117239

Stull, R. B. (1988). *An introduction to boundary layer meteorology*. Springer. https://doi.org/10.1007/978-94-009-3027-8

Su, T., Li, J., Li, C., Xiang, P., Lau, A. K.-H., Guo, J., et al. (2017). An intercomparison of long-term planetary boundary layer heights retrieved from CALIPSO, ground-based Lidar, and radiosonde measurements over Hong Kong. *Journal of Geophysical Research: Atmospheres*, *122*(7), 3929–3943. https://doi.org/10.1002/2016JD025937

Tang, G., Zhang, J., Zhu, X., Song, T., Münkel, C., Hu, B., et al. (2016). Mixing layer height and its implications for air pollution over Beijing, China. *Atmospheric Chemistry and Physics*, *16*(4), 2459–2475. https://doi.org/10.5194/acp-16-2459-2016

Tong, C. H. M., Yim, S. H. L., Rothenberg, D., Wang, C., Lin, C.-Y., Chen, Y. D., & Lau, N. C. (2018). Projecting the impacts of atmospheric conditions under climate change on air quality over the Pearl River Delta region. *Atmospheric Environment*, *193*, 79–87. https://doi.org/10.1016/j.atmosenv.2018.08.053

Tse, L. K. S., Hon, K. K., & Li, L. K. B. (2020). Large-eddy simulations of neutrally stratified airflow over the complex terrain around Hong Kong International Airport with a three-runway system. *Meteorological Applications*, *27*(1), e1847. https://doi.org/10.1002/met.1847

Wang, X., Dickinson, R. E., Su, L., Zhou, C., & Wang, K. (2018). $PM_{2.5}$ pollution in China and how it has been exacerbated by terrain and meteorological conditions. *Bulletin of the American Meteorological Society*, *99*(1), 105–119. https://doi.org/10.1175/BAMS-D-16-0301.1

Yang, D., Li, C., Lau, A. K.-H., & Li, Y. (2013). Long-term measurement of daytime atmospheric mixing layer height over Hong Kong. *Journal of Geophysical Research: Atmospheres*, *118*(5), 2422–2433. https://doi.org/10.1002/jgrd.50251

Yang, Y., Yim, S. H. L., Haywood, J., Osborne, M., Chan, J. C. S., Zeng, Z., & Cheng, J. C. H. (2019). Characteristics of heavy particulate matter pollution events over Hong Kong and their relationships with vertical wind profiles using high-time-resolution Doppler Lidar measurements. *Journal of Geophysical Research: Atmospheres*, *124*(16), 9609–9623. https://doi.org/10.1029/2019JD031140

Yim, S. H. L. (2020). Development of a 3D real-time atmospheric monitoring system (3DREAMS) using Doppler LiDARs and applications for long-term analysis and hot-and-polluted episodes. *Remote Sensing*, *12*(6), 1036. https://doi.org/10.3390/rs12061036

Yim, S. H. L., Gu, Y., Shapiro, M. A., & Stephens, B. (2019). Air quality and acid deposition impacts of local emissions and transboundary air pollution in Japan and South Korea. *Atmospheric Chemistry and Physics*, *19*(20), 13309–13323. https://doi.org/10.5194/acp-19-13309-2019

Yim, S. H. L., Hou, X., Guo, J., & Yang, Y. (2019). Contribution of local emissions and transboundary air pollution to air quality in Hong Kong during El Niño-Southern Oscillation and heatwaves. *Atmospheric Research*, *218*, 50–58. https://doi.org/10.1016/j.atmosres.2018.10.021

Yuval, J., & O'Gorman, P. A. (2020). Stable machine-learning parameterization of subgrid processes for climate modeling at a range of resolutions. *Nature Communications*, *11*(1), 3295. https://doi.org/10.1038/s41467-020-17142-3

Zhang, Y., Guo, J., Yang, Y., Wang, Y., & Yim, S. (2020). Vertical wind shear modulates particulate matter pollutions: A perspective from radar wind profiler observations in Beijing, China. *Remote Sensing*, *12*(3), 546. https://doi.org/10.3390/rs12030546

Zhu, X., Tang, G., Guo, J., Hu, B., Song, T., Wang, L., et al. (2018). Mixing layer height on the North China Plain and meteorological evidence of serious air pollution in southern Hebei. *Atmospheric Chemistry and Physics*, *18*(7), 4897–4910. https://doi.org/10.5194/acp-18-4897-2018

References From the Supporting Information

Bodini, N., Lundquist, J. K., & Newsom, R. K. (2018). Estimation of turbulence dissipation rate and its variability from sonic anemometer and wind Doppler Lidar during the XPIA field campaign. *Atmospheric Measurement Techniques*, *11*(7), 4291–4308. https://doi.org/10.5194/amt-11-4291-2018

Chan, P. W., Hon, K. K., & Li, Q. S. (2020). A comprehensive study of terrain-disrupted airflow at Hong Kong International Airport—Observations and numerical simulations. *Weather*, *75*(7), 199–206. https://doi.org/10.1002/wea.3593

Ciofini, M., Lapucci, A., & Lolli, S. (2003). Diffractive optical components for high power laser beam sampling. *Journal of Optics A: Pure and Applied Optics*, *5*(3), 186–191. https://doi.org/10.1088/1464-4258/5/3/308

Hon, K. K., & Chan, P. W. (2014). Application of LIDAR-derived eddy dissipation rate profiles in low-level wind shear and turbulence alerts at Hong Kong International Airport. *Meteorological Applications*, *21*(1), 74–85. https://doi.org/10.1002/met.1430

Hon, K.-K., & Chan, P.-W. (2020). Alerting of hectometric turbulence features at Hong Kong International airport using a short-range LIDAR. *Meteorological Applications*, *27*(5). https://doi.org/10.1002/met.1945

Lolli, S., Delaval, A., Loth, C., Garnier, A., & Flamant, P. H. (2013). 0.355-micrometer direct detection wind Lidar under testing during a field campaign in consideration of ESA's ADM-Aeolus mission. *Atmospheric Measurement Techniques*, *6*(12), 3349–3358. https://doi.org/10.5194/amt-6-3349-2013

Manninen, A. J., Marke, T., Tuononen, M., & O'Connor, E. J. (2018). Atmospheric boundary layer classification with Doppler Lidar. *Journal of Geophysical Research: Atmospheres*, *123*(15), 8172–8189. https://doi.org/10.1029/2017JD028169

O'Connor, E. J., Illingworth, A. J., Brooks, I. M., Westbrook, C. D., Hogan, R. J., Davies, F., & Brooks, B. J. (2010). A method for estimating the turbulent kinetic energy dissipation rate from a vertically pointing Doppler Lidar, and independent evaluation from balloon-borne in situ measurements. *Journal of Atmospheric and Oceanic Technology*, *27*(10), 1652–1664. https://doi.org/10.1175/2010JTECHA1455.1

Shun, C. M., & Chan, P. W. (2008). Applications of an Infrared Doppler Lidar in detection of wind shear. *Journal of Atmospheric and Oceanic Technology*, *25*(5), 637–655. https://doi.org/10.1175/2007JTECHA1057.1

Tonttila, J., O'Connor, E. J., Hellsten, A., Hirsikko, A., O'Dowd, C., Järvinen, H., & Räisänen, P. (2015). Turbulent structure and scaling of the inertial subrange in a stratocumulus-topped boundary layer observed by a Doppler Lidar. *Atmospheric Chemistry and Physics*, *15*(10), 5873–5885. https://doi.org/10.5194/acp-15-5873-2015

Wang, L., Wang, H., Liu, J., Gao, Z., Yang, Y., Zhang, X., et al. (2019). Impacts of the near-surface urban boundary layer structure on PM$_{2.5}$ concentrations in Beijing during winter. *The Science of the Total Environment*, *669*, 493–504. https://doi.org/10.1016/j.scitotenv.2019.03.097

Wu, T.-C., & Hon, K.-K. (2018). Application of spectral decomposition of LIDAR-based headwind profiles in windshear detection at the Hong Kong International Airport. *Meteorologische Zeitschrift*, *27*, 33–42. https://doi.org/10.1127/metz/2017/0858

Yim, S. H. L. (2020). Development of a 3D real-time atmospheric monitoring system (3DREAMS) using Doppler LiDARs and applications for long-term analysis and hot-and-polluted episodes. *Remote Sensing*, *12*(6). https://doi.org/10.3390/rs12061036